Lithography

DOI: 10.1002/anie.200804171

Direct Fabrication of 3D Periodic Inorganic Microstructures using Conformal Phase Masks**

*Matthew C. George, Erik C. Nelson, John A. Rogers, and Paul V. Braun**

Three-dimensional micro- and nanofabricated structures have numerous applications in photonics,[1] microfluidics,[2,3] tissue engineering,[4,5] drug delivery,[4,5] chemical detection,[6,7] energy and data storage,[8–10] and as catalyst supports.[11] Many serial techniques exist for micro- and nanofabrication, including layer-by-layer photolithographic approaches,[12,13] nanotransfer printing,[14] microstereolithography,[15] multiphoton polymerization,[16] and ink-based direct-write assembly,[17,18] but high cost and slow patterning speeds make industrial scale-up difficult. Self-assembly techniques provide rapid routes to form large-area micro- and nanostructures, but they suffer from poor control over defect density and limited flexibility in the types of structures that can be fabricated.[19] Interference lithography (IL), which relies on the interference of multiple coherent beams of light, is a popular choice to fabricate nearly defect-free 1D, 2D, and 3D periodic microstructures over large areas using one or more parallel exposures.[19] By tuning the number of laser beams and their relative orientation, intensity, and polarization, IL offers great flexibility in the types of periodic lattices and structural motifs that can be formed.[20] IL can be combined with micromolding techniques,[21] stop-flow lithography,[22] and multiphoton lithography[23,24] to further expand on the types of structures that can be fabricated. To fabricate structures with high precision, IL is typically limited to organic photoresists. Unfortunately, the structures formed using these organic materials generally lack structural stability at high temperatures. They often require additional time-consuming processing steps to make them more robust for real-world applications,[25,26] often with loss of fidelity during processing.

[*] M. C. George, E. C. Nelson, Prof. J. A. Rogers, Prof. P. V. Braun
Frederick Seitz Materials Research Laboratory
Department of Materials Science and Engineering
University of Illinois at Urbana-Champaign, Urbana, IL 61801 (USA)
Fax: (+1) 217-333-2736
E-mail: pbraun@illinois.edu

[**] We thank Dr. S. Jeon and Prof. D. G. Cahill for helpful discussions and Dr. M. J. Highland, D. Shir, Y. C. Chen, T. D. Gould, J. Achilles, and A. Jerez for technical assistance. PMSSQ photoresist development was supported by US Army Research Office grant DAAD19-03-1-0227, and PnP patterning of PMSSQ was supported by the US Department of Energy, Division of Materials Sciences grant DE-FG02-07ER46471, through the Frederick Seitz Materials Research Laboratory at the University of Illinois at Urbana-Champaign. This work was carried out in part in the Center for Microanalysis of Materials, University of Illinois, which is partially supported by the US Department of Energy under grants DE-FG02-07ER46453 and DE-FG02-07ER46471.

Supporting information for this article is available on the WWW under http://dx.doi.org/10.1002/anie.200804171.

We report for the first time a silsesquioxane-based photoresist that is compatible with 3D interference lithography and offers many of the same advantages of organic photoresists, including sub-micrometer resolution, but with material properties more amenable to post-fabrication processing, such as improved thermal stability and resistance to reactive-ion etching.[27–30] The photoresist is based on the acid-catalyzed cross-linking of poly(methylsilsesquioxane) (PMSSQ; Scheme 1c). PMSSQ is a well-known spin-on glass used in microfabrication owing to its low dielectric constant and compatibility with standard semiconductor processing techniques. It also has excellent transparency over a broad spectral range (230 nm to 2.68 μm). Moreover, PMSSQ has good solubility in both organic solvents and aqueous bases, allowing for spin-coating and standard wet development. The acid-catalyzed cross-linking enables chemical amplification for heightened sensitivity. The cross-linked resin is extremely hydrophobic and even resists aqueous bases, enabling a strong change in solubility that limits feature swelling and distortion during development.[30] Finally, PMSSQ can be converted into a silica-like material, allowing for facile removal by HF etching.[27,28] These properties make PMSSQ resist structures ideal templates for the patterning of secondary materials for photonic and optoelectronic applications.

The other components of our PMSSQ photoresist include a photosensitizer that absorbs radiation at the relevant exposure wavelength and a photoacid generator (PAG), which oxidizes the excited photosensitizer (or reactive intermediate) and decomposes into a strong acid (Scheme 1b). The photosensitizer is isopropylthioxanthone (ITX), a common hydrogen-abstraction initiator that absorbs in the UV range ($\lambda_{max} = 384$ nm) and exhibits two-photon absorption in the near-IR region.[31,32] We chose *p*-cumyl-*p*-tolyliodonium tetrakis(pentafluorophenyl)borate (Rhodorsil 2074) as the PAG, as it has good solubility in silsesquioxane resins and forms a strong acid ($pK_a \approx -16$)[33] containing the large tetrakis(pentafluorophenyl)borate counterion. This system showed improved sensitivity and contrast, presumably owing to its high reactivity and a reduced acid diffusion rate.[34]

The general form of IL used herein is termed proximity-field nanopatterning (PnP), which typically consists of an elastomeric phase mask placed in conformal contact with the surface of a photoresist.[35] Upon exposure, diffraction from the conformal phase mask generates interfering beams within the photoresist material (see Figure S1 in the Supporting Information). The advantages of PnP over multibeam IL include a simpler setup (single, self-aligning optical element and single-beam exposure) and reduced coherence require-

 InterScience © 2009 Wiley-VCH Verlag GmbH & Co. KGaA, Weinheim

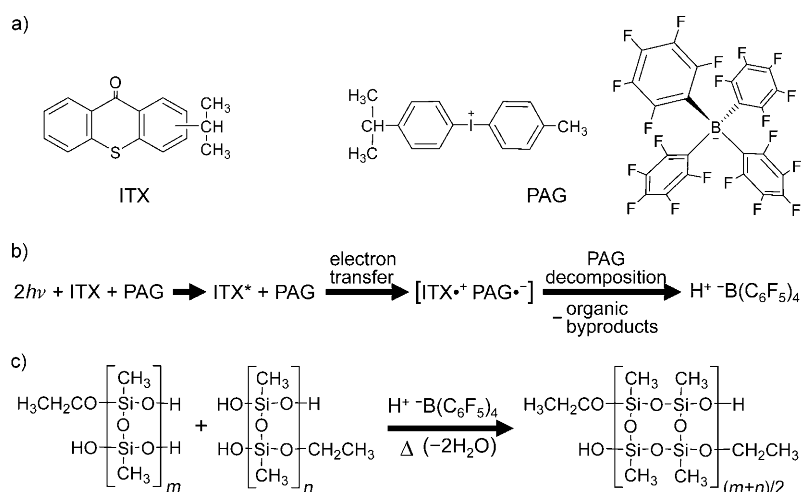

Scheme 1. a) Photoactive compounds: sensitizer (ITX) and photoacid generator (PAG). b) Photoacid generation process. c) Acid-catalyzed cross-linking of poly(methylsilsesquioxane).

ments owing to the photoresist's proximity to a single common beam-splitting element, which allows for flexibility in exposure sources, including improved compatibility with ultrashort pulsed lasers as compared to multibeam IL.[36] The compatibility of PnP with ultrashort pulsed lasers allows patterning at much longer wavelengths by two-photon absorption, in a process termed two-photon PnP.[23] This longer wavelength patterning is important, because it enlarges the allowable characteristic feature size of the phase mask necessary to fabricate a given class of structures. It also results in an improved image contrast, because second-order absorption processes, which depend on the square of the intensity, are responsible for generating the 3D latent images in the photoresist.[23] These two effects (longer-wavelength exposure and nonlinear absorption) ease the resolution requirements of the photoresist. Also, since it is the exposure wavelength within the photoresist that determines the structure for a given phase mask, the PMSSQ material has an additional advantage over traditional organic thick-film photoresists (such as SU-8). This advantage stems from PMSSQ's lower index of refraction (n) and larger effective exposure wavelength in the near-IR region ($n_{PMSSQ} = 1.434$, $n_{SU\text{-}8} = 1.58$), which for a given target structure allows for a further 10% relaxation of the resolution requirements for both phase-mask fabrication and photoresist patterning.

The PMSSQ resist is also compatible with maskless PnP, which uses a micromolding technique (also known as nanoimprint lithography) to emboss the phase-shifting element into the surface of the photoresist (Figure 1 a–c). Upon exposure to a narrow-band light source, this surface relief structure generates diffracted beams at well-defined angles (Figure 1 d), which produces a 3D periodic interference pattern within the photoresist. Two-photon absorption within the interference pattern generates a 3D periodic acid distribution (Scheme 1 b). Post-exposure baking then catalyzes the silanol condensation (Scheme 1 c), which selectively increases the molecular weight in regions of the interference pattern that contained higher light intensities. Development (etching) in aqueous base removes the lower molecular weight material, and upon rinsing and drying, a periodic microstructure is left behind, as seen in the SEM micrographs in Figure 1 e–g. The fabricated microstructures closely resemble the results of modeling (see insets) based on rigorous coupled wave analysis (RCWA) and the principal of superposition, where a threshold has been applied such that the high-intensity regions (corresponding to polymer) are depicted in blue.

One advantage of maskless PnP is the improved image contrast at small grating relief depths compared to the conformal phase mask case, in which the grating relief depth is simply equal to the cylindrical post height of the mask or mold. Previously, this improved contrast was attributed to the larger phase modulation in the maskless case, which arises from a larger index mismatch between grating materials ($\Delta n = 0.58$ for the organic photoresist SU-8 and air; $\Delta n \approx 0.4$ for PDMS and air).[21] However, the same behavior can be seen when using this PMSSQ resist system, which has a refractive index nearly identical to that of PDMS

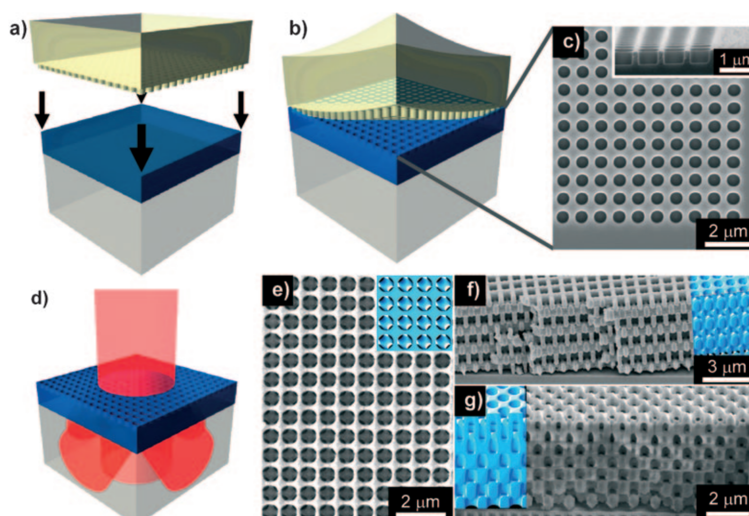

Figure 1. Maskless PnP process for the fabrication of 3D periodic microstructures. a), b) Schematic views of the micromolding process using an elastomeric PDMS stamp. c) Plan-view SEM image and cleaved cross-section (inset) of the micromolded PMSSQ photoresist surface relief structure. d) Exposure through the relief structure generates diffracted beams for maskless PnP, which upon post-baking and development generates 3D periodic PMSSQ microstructures. SEM images of e) plan view, f) {100} cleaved section, g) focused ion beam milled cross-section (ca. {110}). The blue insets represent modeling of the structure on the basis of a threshold approximation of the intensity-squared distribution assuming circularly polarized, 800 nm exposure wavelength, and the following imprint design: 760 nm pitch square array of cylindrical holes with 305 nm radius and 400 nm relief depth.

 © 2009 Wiley-VCH Verlag GmbH & Co. KGaA, Weinheim

at 800 nm ($n = 1.434$ vs. $n \approx 1.4$). To understand this effect, it is useful to examine the relative strength of the beams that are transmitted into the resist. The four-fold rotational and mirror symmetries of the grating design, coupled with the exposure conditions (circular polarization), generates four first-order diffracted beams of equal intensity that are transmitted into the resist.[23,37] These beams interfere with each other and with the zero-order transmitted beam to form the 3D periodic intensity distribution within the resist. If the relative strength in the first-order beams is too low compared to the zero-order beam, the intensity distribution will have weak modulation, giving poor patterning results. Figure 2a compares the relative strength of the first-order to zero-order beams (diffraction efficiency ratio D_{10}/D_{00}) for the conformal and maskless PnP cases at two different grating periods, $a = 710$ and 760 nm. A significant enhancement for maskless PnP exists at all but the largest relief depths (see the Supporting Information). This enhancement is also readily apparent in Figure 2b, which depicts the diffraction efficiency ratio versus the grating period at a fixed, experimentally relevant relief depth of 400 nm. The best grating period for producing 3D periodic structures by maskless PnP appears to lie in the 740–760 nm range for our system. The high-quality results presented in Figure 1 were obtained in this optimal range.

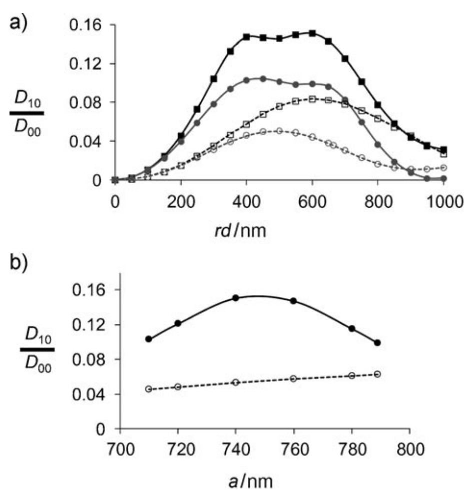

Figure 2. Diffraction efficiency ratio D_{10}/D_{00} vs. a) relief depth *rd* for grating periods of 760 nm (black squares) and 710 nm (gray circles) and b) grating period *a* for $rd = 400$ nm. a),b) -----: conformal PnP; ——: maskless PnP. The ratio D_{10}/D_{00} describes the relative power of the first-order to zero-order transmitted beams and is used as a simple figure of merit for PnP.

Comparison of measured and predicted optical properties is another way to probe the quality of the microstructured PMSSQ. Figure 3 depicts the reflectance spectrum taken in the [001] crystal direction (normal incidence) and compares it to the reflectance spectrum calculated from a model structure using the finite difference time domain (FDTD) method. The structure used in the FDTD calculation utilizes a threshold approximation in which regions of the intensity distribution below the intensity threshold are assumed to be completely removed during development and regions above the threshold are given the PMSSQ optical constants. The chosen intensity threshold ($I^2 = 0.5$) gives a 3D structure with a polymer fill factor of 53%; on the basis of the SEM cross-sections of Figure 1 f,g, the simulated structure contains 3.5 unit cells in the [001] direction. Figure 3 shows good agreement in the high-energy peak positions, although there is broadening and a reduced reflectance in the experimental measurements (see the Supporting Information). The low-energy peak, associated with the layer spacing in the z dimension, occurs at about 2.1 μm but is strongly suppressed. Figure S3 in the Supporting Information shows the effects of varying the intensity threshold on the modeled unit cell and on the low-energy peak predicted by FDTD calculation. This peak, which results from a pseudo-gap along the [001] crystal direction, is suppressed at the experimentally relevant fill fractions of 40–55%. However, a relatively thick film of 13.5 unit cells would give a more substantial reflectance (ca. 43%, see Figure S4 in the Supporting Information). Thicker photonic crystal films would give larger reflectance peaks, but even upon inversion into silicon, the resulting structure does not exhibit a full photonic band gap. The lack of a full band gap is not surprising, as the chosen grating period ($a \approx 740$–760 nm) produces an elongated body-centered tetragonal unit cell with $a/c \approx 0.446$ (the grating period a is equal to the standard lateral lattice parameter of the unit cell, and c is the corresponding axial parameter), whereas face-centered cubic (fcc) symmetry requires $a/c = 0.707$. Obtaining this symmetry, which is useful for generating large, full photonic band gaps upon silicon inversion,[38] requires a phase mask of 592 nm periodicity for an 800 nm wavelength exposure in PMSSQ. Unfortunately, these exposure conditions result in reduced image contrast for typical phase-mask designs. When coupled with the reduced lattice parameter, this reduced contrast places stricter resolution requirements on the photoresist than have been met to date. Potential routes towards fcc PMSSQ photonic crystals include advances in phase-mask design and longer-wavelength exposure conditions.

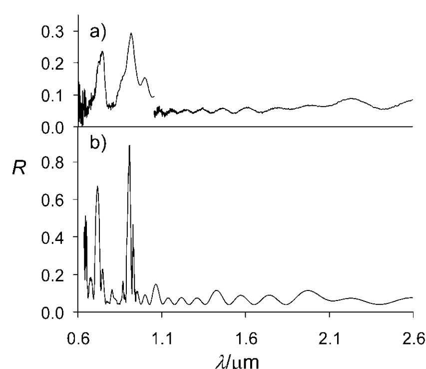

Figure 3. Comparison of a) the experimentally measured reflectance R to b) the reflectance calculated by finite difference time domain simulation for a PMSSQ crystal 3.5 unit cells thick and fabricated by maskless PnP (as depicted in Figure 1 e–g).

In addition to photonic crystals, many other novel structures can be fabricated with PMSSQ photoresists using PnP techniques, such as fibers, helical arrays, and colloids of

 © 2009 Wiley-VCH Verlag GmbH & Co. KGaA, Weinheim

various shapes, including ellipsoid, helical, and cuboid-like particles. Figure 4 depicts example structures fabricated by maskless PnP (Figure 4a) and conformal PnP (Figure 4b–e).

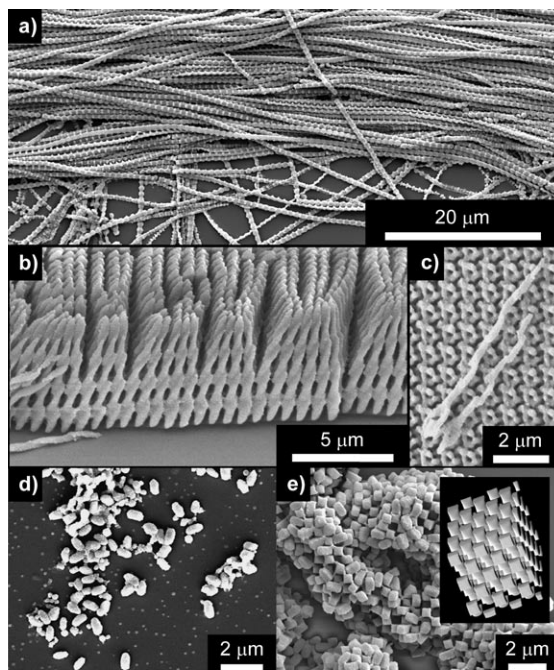

Figure 4. SEM images of a large variety of structures fabricated by PnP: a) fibers, b), c) helix-like arrays and particles, and aggregated colloidal particles of d) ellipsoids and e) rounded cuboids. The inset in (e) depicts thresholded modeling.

The colloidal particles are formed using typical conformal PnP, but with exposure conditions that allow for isolated particles upon development. Figure 4e presents cuboid-like colloids that have not yet been completely etched into isolated particles. The helices and fibers are formed using asymmetric beam configurations. These configurations are achieved by simply eliminating or diminishing certain diffracted orders from the photoresist by backside exposure through the substrate or by changing the incoming polarization from circular to elliptical. Inverse design of the phase mask and incoming polarization conditions can also be utilized to produce these and other types of exotic structures,[39] with potential applications in photonics,[37,40,41] chemical detection,[6,7] drug delivery,[4,5] microfluidics,[2,3] and catalysis.[11]

In conclusion, we have developed a primarily inorganic photoresist that is compatible with 3D interference lithography. The photoresist displays sub-micrometer resolution and is based on poly(methyl silsesquioxane), which has distinct advantages over traditional thick-film organic photoresists, including improved transparency and relaxed PnP resolution constraints. Furthermore, its material properties are more amenable to post-fabrication processing. For example, it has good thermal stability and is resistant to reactive-ion etching. Deficiencies in the PMSSQ resist system have been limited by careful choice of PAG and developer and by utilization of two-photon PnP and maskless PnP. These results should expand the types of materials that can be patterned using interference lithography by templating while reducing processing complexity.

Experimental Section

Details of the fabrication of conformable poly(dimethylsiloxane) (PDMS) phase masks are given in reference [35].

PMSSQ photoresist film formation: The PMSSQ resin was synthesized according to reference [35] with modifications (see the Supporting Information). Cyclopentanone solutions containing 5–15 wt% PAG (Rhodorsil 2074, Rhodia Inc.) and photosensitizer (Darocure ITX, Ciba Specialty Chemicals Inc.) were added to the PMSSQ resin such that the PAG comprised 0.8–1.2% of the total solid content and the molar ratio of sensitizer to PAG was 1.0–1.4. Photoresist solutions were refrigerated until use and could be stored for up to five months without significant degradation in the ability to be patterned by PnP. Photoresist solutions were deposited onto clean glass or fused silica substrates (see the Supporting Information for the cleaning procedure) through a 0.22 or 0.45 μm teflon syringe filter and spin-coated for 30 s at 2000 rpm after a gradual ramp-up to give transparent but tacky films. The samples were then pre-exposure baked on a hotplate at 65, 95, and 65 °C for 5–15, 10–20, and 5–10 min respectively (longer pre-bake times for thicker films), giving tack-free, transparent films upon cooling. The index of refraction of PMSSQ films without photoactive components was measured using spectroscopic ellipsometry (VASE, J. A. Woollam Co.). At the typical exposure conditions ($\lambda = 800$ nm), $n_{PMSSQ} = 1.4342$. Fitting the dispersion curve gave Cauchy coefficients of 1.434, -9.87×10^{-4}, and 7.33×10^{-4} for A_n, B_n, and C_n respectively.

PMSSQ resist micromolding: See the Supporting Information for details.

Proximity-field nanopatterning: One-photon PnP: After bringing the PDMS phase mask into contact with the back of the glass substrate, a block of PDMS was placed on top of the resist surface to couple out transmitted beams. The PMSSQ resist was exposed for 10–20 s through the phase mask using an argon ion laser (Coherent, Inc.) operating at 351 nm (linear polarization) with a beam diameter of 3.7 mm and at a power of 14.5–16.0 mW.

Two-photon PnP: Circularly polarized light from a regeneratively amplified Ti:sapphire laser (Spectra-Physics, Spitfire-Pro) operating at a wavelength of 800 nm with a pulse energy of 1.8–2.0 mJ, a repetition rate of 1 kHz, and a pulse width of 120–145 fs was focused to a diameter ($2w_0$) of 7.8–12 mm for a peak fluence of $2.6–6.9\times10^{10}$ $W\,cm^{-2}$ using a 400 mm focal length lens. For maskless PnP (Figure 1), imprinted samples were exposed directly to the beam described above, while for conformal PnP samples (Figure S1 in the Supporting Information), PDMS phase masks were brought into contact with the smooth PMSSQ resist surface before exposure through the mask. Exposure times ranged from 45 to 120 s and were dependent on the beam and phase-mask parameters and the version of PnP being utilized. After a 5–6 min, 65 °C post-exposure bake on a hotplate, samples were developed using aqueous tetramethylammonium hydroxide (TMAH) solutions with concentrations ranging from 5–10 wt%. Development times ranged from 60 s for strong TMAH concentrations to 5 min for weaker TMAH concentrations. Samples were rinsed for 60 and 30 s in separate baths of deionized water and dried slowly in air or with a gentle nitrogen stream.

Sample characterization: Reflectance spectra were recorded with a Fourier transform infrared (FTIR) spectrometer attached to a microscope (Bruker Vertex 70 and Hyperion 2000, respectively) using a 4×, 0.1 NA glass (or custom 2.4×, 0.07 NA CaF_2) objective and a spatial aperture to limit the collection area to a diameter of 112.5 μm for the visible to near-IR scan (125 μm for the mid-IR scan). The light source was unpolarized. Sample cross-sections were formed by cleavage and by focused ion beam milling (FEI Dual Beam 235

 © 2009 Wiley-VCH Verlag GmbH & Co. KGaA, Weinheim

FIB). Sample morphology was characterized using a scanning electron microscope (Philips XL30 ESEM-FEG) after deposition of approximately 10 nm of Au or Au–Pd by sputtering.

Modeling and simulation: See the Supporting Information for details.

Received: August 23, 2008
Published online: December 3, 2008

Keywords: nanoimprinting · nanolithography · photochemistry · silsesquioxanes

[1] E. Yablonovitch, *J. Mod. Opt.* **1994**, *41*, 173.
[2] D. Therriault, S. R. White, J. A. Lewis, *Nat. Mater.* **2003**, *2*, 265.
[3] S. Jeon, V. Malyarchuk, J. O. White, J. A. Rogers, *Nano Lett.* **2005**, *5*, 1351.
[4] A. delCampo, E. Arzt, *Chem. Rev.* **2008**, *108*, 911.
[5] E. Fabrizio, F. Perennes, F. Romanato, S. Cabrini, D. Cojoc, M. Tormen, L. Businaro, L. Vaccari, R. Proietti, R. Kumar, *BioMEMS Nanotechnol.* **2006**, p. 97.
[6] X. Hu, G. Li, M. Li, J. Huang, Y. Li, Y. Gao, Y. Zhang, *Adv. Funct. Mater.* **2008**, *18*, 575.
[7] J. H. Holtz, S. A. Asher, *Nature* **1997**, *389*, 829.
[8] J. W. Long, B. Dunn, D. R. Rolison, H. S. White, *Chem. Rev.* **2004**, *104*, 4463.
[9] L. Dhar, K. Curtis, T. Facke, *Nat. Photonics* **2008**, *2*, 403.
[10] D. A. Parthenopoulos, P. M. Rentzepis, *Science* **1989**, *245*, 843.
[11] M. L. K. Hoa, M. Lu, Y. Zhang, *Adv. Colloid Interface Sci.* **2006**, *121*, 9.
[12] S. Noda, N. Yamamoto, H. Kobayashi, M. Okano, K. Tomoda, *Appl. Phys. Lett.* **1999**, *75*, 905.
[13] P. Yao, G. Schneider, D. Prather, E. Wetzel, D. O'Brien, *Opt. Express* **2005**, *13*, 2370.
[14] J. Zaumseil, M. A. Meitl, J. W. P. Hsu, B. R. Acharya, K. W. Baldwin, Y. L. Loo, J. A. Rogers, *Nano Lett.* **2003**, *3*, 1223.
[15] P. Dario, M. C. Carrozza, N. Croce, M. C. Montesi, M. Cocco, *J. Micromech. Microeng.* **1995**, *5*, 64.
[16] G. Witzgall, R. Vrijen, E. Yablonovitch, V. Doan, B. J. Schwartz, *Opt. Lett.* **1998**, *23*, 1745.
[17] J. E. Smay, G. M. Gratson, R. F. Shepherd, J. Cesarano, J. A. Lewis, *Adv. Mater.* **2002**, *14*, 1279.
[18] E. B. Duoss, M. Twardowski, J. A. Lewis, *Adv. Mater.* **2007**, *19*, 3485.
[19] J. H. Moon, J. Ford, S. Yang, *Polym. Adv. Technol.* **2006**, *17*, 83.
[20] A. J. Turberfield, *MRS Bull.* **2001**, *26*, 632.
[21] S. Jeon, D. J. Shir, Y. S. Nam, R. Nidetz, M. Highland, D. G. Cahill, J. A. Rogers, M. F. Su, I. F. El-Kady, C. G. Christodoulou, G. R. Bogart, *Opt. Express* **2007**, *15*, 6358.
[22] J.-H. Jang, D. Dendukuri, T. A. Hatton, E. L. Thomas, P. S. Doyle, *Angew. Chem.* **2007**, *119*, 9185; *Angew. Chem. Int. Ed.* **2007**, *46*, 9027.
[23] S. Jeon, V. Malyarchuk, J. A. Rogers, G. P. Wiederrecht, *Opt. Express* **2006**, *14*, 2300.
[24] J. Scrimgeour, D. N. Sharp, C. F. Blanford, O. M. Roche, R. G. Denning, A. J. Turberfield, *Adv. Mater.* **2006**, *18*, 1557.
[25] J. S. King, E. Graugnard, O. M. Roche, D. N. Sharp, J. Scrimgeour, R. G. Denning, A. J. Turberfield, C. J. Summers, *Adv. Mater.* **2006**, *18*, 1561.
[26] V. Ramanan, E. Nelson, A. Brzezinski, P. V. Braun, P. Wiltzius, *Appl. Phys. Lett.* **2008**, *92*, 173304.
[27] Y. Jun, C. A. Leatherdale, D. J. Norris, *Adv. Mater.* **2005**, *17*, 1908.
[28] Y. Jun, P. Nagpal, D. J. Norris, *Adv. Mater.* **2008**, *20*, 606.
[29] D. R. McKean, N. J. Clecak, L. A. Pederson, *Advances in Resist Technology and Processing VII*, *Vol. 1262*, 1st ed., SPIE, San Jose, CA, **1990**, p. 110.
[30] H. Watanabe, Y. Todokoro, M. Inoue, *Microelectron. Eng.* **1991**, *13*, 69.
[31] K. D. Belfield, K. J. Schafer, Y. Liu, J. Liu, X. Ren, E. W. Van Stryland, *J. Phys. Org. Chem.* **2000**, *13*, 837.
[32] Y. Boiko, J. Costa, M. M. Wang, S. Esener, *Opt. Express* **2001**, *8*, 571.
[33] M. G. Cupta, Masters thesis, Georgia Institute of Technology (Atlanta), **2006**.
[34] X. Shi, *J. Vac. Sci. Technol. B* **1999**, *17*, 350.
[35] S. Jeon, J.-U. Park, R. Cirelli, S. Yang, C. E. Heitzman, P. V. Braun, P. J. A. Kenis, J. A. Rogers, *Proc. Natl. Acad. Sci. USA* **2004**, *101*, 12428.
[36] K. Toshiaki, J. Saulius, M. Vygantas, M. Shigeki, M. Hiroaki, *New J. Phys.* **2006**, *9*, 250.
[37] T. Y. M. Chan, O. Toader, S. John, *Phys. Rev. E* **2006**, *73*, 046610.
[38] K. Busch, S. John, *Phys. Rev. E* **1998**, *58*, 3896.
[39] J. W. Rinne, S. Gupta, P. Wiltzius, *Opt. Express* **2008**, *16*, 663.
[40] A. Chutinan, S. Noda, *Phys. Rev. B* **1998**, *57*, R2006.
[41] M. Thiel, M. Hermatschweiler, M. Wegener, G. von Freymann, *Appl. Phys. Lett.* **2007**, *91*, 123515.

 © 2009 Wiley-VCH Verlag GmbH & Co. KGaA, Weinheim